Atomistic simulations of pristine and defective hexagonal BN and Sic sheets under uniaxial tension The uniaxial tensile mechanical properties of pristine and defective hexagonal boron nitride (BN) and silicon carbide (SiC) sheets are investigated through a molecular dynamics finite element method with Tersoff and Tersoff-like potentials. 2-	Mô phỏng cấp độ nguyên tử các tấm BN và SiC lục giác nguyên sơ và khuyết tật dưới tác dụng của ứng suất đơn trục Chúng tôi khảo sát các tính chất cơ học kéo đơn trục của các tấm Bo Nitrit (BN) và silicon carbide (SiC) bằng phương pháp phần tử hữu hạn động học phân tử, phương pháp này sử dụng các thế Tersoff và tương tự Tersoff. Chúng ta sẽ xét các sai hỏng khuyết 2

Atom vacancy and 2 types of Stone-Wales defects are considered. It is found that uniaxial tensile stress-strain curves of defective and pristine sheets are almost identical up to fracture points. A centered single defect reduces significantly fracture stress and fracture strain from those of the corresponding pristine sheet. In contrast, Young's modulus is nearly unchanged by a single defect. One 2-atom vacancy in the sheet's center reduces 15-18% and 16-25% in fracture stress, and 32-34% and 32-48% in fracture strain of BN and SiC sheets, respectively. Reduction in fracture properties depends on the tensile direction as well as the orientation of Stone-Wales defects.

nguyên tử và hai loại sai hỏng Stone-Wales. Chúng tôi nhận thấy rằng đường cong ứng suất-biến dạng kéo đơn trục của các tấm nguyên sơ và sai hỏng hầu như gần giống hệt nhau cho đến tận các điểm gãy. Các tấm bị sai hỏng đơn trung tâm có ứng suất gãy và biến dạng gãy giảm đáng kể so với các tấm nguyên sơ tương ứng. Trái lại, suất Young gần như không thay đổi trong sai hỏng đơn. Chổ khuyết 2 nguyên tử ở tâm của các tấm BN và SiC lần lượt có ứng suất gãy giảm 15-18% và 16-25%, và có biến dạng gãy giảm 32-34% và 32-48%. Sự giảm gãy phụ thuộc vào hướng kéo cũng như sự định hướng của các khuyết tật Stone-Wales.

1. Introduction

Two-dimensional (2D) hexagonal boron nitride (BN) and silicon carbide (SiC) sheets exhibit a honeycomb lattice structure with an analog of graphene and have been recently synthesized; see e.g. [1-4]. While graphene is well known as a zero band gap semimetal, both BN and SiC sheets exhibit a finite band-gap semiconductor with capacity of ultraviolet light-emission [2,4-6]. Therefore, these 2 low-dimensional materials promise many potential applications, espe-cially in optoelectronic nanodevices.

In terms of mechanical characterization, BN sheets and nanotubes have been investigated both by theoretical work such as density functional theory (DFT) calculations [7-13], and molecular dynamics (MD) simulations [14-21] and by experiments [3,22-25]. Research on mechanical properties of SiC sheets and nanotubes have been also reported [8,9,12,21,26]. However, most of

above-cited work focused on elastic properties of these 2 sheets, their nanoribbons and their nanotubes. It should be noted that recent MD simulations [18-20] with Tersoff and Tersoff-like potentials would overestimate the fracture stress and fracture strain of BN sheets due to the problem of the cutoff function as noted in Section 2.2. Using DFT calculations, Topsakal and Ciraci [10] indicated that armchair BN nanoribbons exhibit non-linear elastic up to an ultimate strain of about 21%, and then the BN nanoribbons are plastically deformed and broken. Based on DFT calculations, Peng et al. [11] proposed a non-linear continuum model for BN sheet. They showed that BN sheet experiences a non-linear elastic deformation up to an ultimate strength followed by a strain softening to the failure.

The Stone-Wales defects and missing atoms (or vacancy), schema-tically shown in Fig. 1, affect significantly the magnetic and electronic properties of BN [27-29] and SiC nanoribbons [30-32]. However, it can be seen from the literature that less work has focused on the mechanical performance of BN and SiC defective sheets.

The main goal of the present study is to investigate mechanical properties of BN and SiC sheets containing such defects. The molecular dynamics finite element method (MDFEM) with Tersoff and Tersoff-like potentials is used. The robustness of the MDFEM is verified by comparing mechanical properties obtained by MDFEM with those by MD

simulations using the same force field parameters for the pristine sheets. This MDFEM is then explored to investigate uniaxial tensile mechanical properties of defective sheets. Effects of the Stone-Wales defects and vacancy are studied and discussed.

2. Framework for analysis

2.1. Interatomic potentials

Tersoff potentials are used to model the interatomic interac-tions [33]. The potential energy E of the atomic structure is a

Fig. 1. Schematic illustration of a planar hexagonal sheet with 2 atom types. (a) A bond (initially parallel to the armchair direction, drawn in red) rotates by 90° to the SWl defect; (b) a bond (initially makes an angle of 30° with the zigzag direction, drawn in red) rotates by 90° to the SW2 defect; (c) a 2-atom vacancy; (d) uniaxial tension. (For interpretation of the references to color in this figure legend, the reader is referred to the web version of this article.)

We denote

Eq. (1c) can be expressed in an alternative form as below

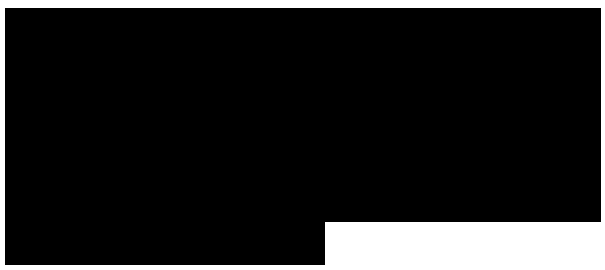

Force field parameters are taken from the work by Sevik et al. [34] and by Erhart and Albe [35] for B-N, and Si—C interactions, respectively. Potentials for Si—C interactions are given as below [35]

Potentials for Si—C interactions [35] take the functional form of the Tersoff potential [33] with

2.2. Cutoff function

It is well known that overestimation of

the maximum force needed to break an interatomic bond is caused by the cutoff function, Eq. (1c); see e.g. [36]. It leads consequently to an overestimation of stress and strain in atomic structures simulated by the Tersoff—Brenner [36—38] and REBO [39] potentials, which employed the same cutoff function, Eq. (1c), suggested by Tersoff [33]. Fig. 2 compares the B—N interatomic stretching energy and force with the original and removed cutoff function in Tersoff potential [34]. When using the original cutoff regime in Eq. (1c), namely the small and large cutoff distances are taken as Rij and Sij, respectively, the tensile bond force rises sharply with a peak at a bond strain of ~35% for B—N interactions. This strange feature in the force was well indicated by Belytschko et al. [36] for C—C interactions with the Brenner potential. Due to this reason, recent MD simulations with Tersoff and Tersoff-like potentials would overestimate the fracture stress and strain of BN sheets [18—20].

In order to avoid the overestimation caused by the original cutoff function, a number of work in the literature have taken the small cutoff distance as the large one (Rij= Sij), as suggested by Refs. [38—41]. It should be noted that when the small cutoff distance is extended to the large one, the cutoff function is shifted to a bond strain less than 50% (about 39% for B—N interactions with Tersoff potential by Sevik et al. [34], 45% for Si—C interactions with

Fig. 2. Evolution of the potential energy (top) and the force (bottom) versus bond strain with the bond angle kept constant according to the Tersoff potential for

B—N interactions [34].
Tersoff-like potential by Erhart and Albe [35], and 46% and 44% for C—C interactions with Tersoff potential [33] and REBO potential [42], respectively); whereas Belytschko et al. [36] have found that the cutoff affects fracture behavior even when it is shifted to 100% strain.
In the present study, the cut-off function is removed from Eq. (1a), fC(rj) = 1 for the whole range of rij. A bond list is created for the initial system and is left unchanged during the simulations. This method was suggested by Shenderova et al. [37] and later adopted by several authors [43—45].

2.3. Molecular dynamics finite element procedure

While experiments are still difficult at nanoscale, computa-tional methods play an important role to explore multi-physical properties of nanostructured materials. Advanced computational techniques such as DFT calculations and MD simulations are time-consuming. Molecular dynamic finite element methods, sometime known as atomic-scale finite element methods or atomistic finite element methods, have been developed to analyze nanostructured materials in a computationally efficient way [46—50]. In MDFEM, atoms and atomic displacements are considered as nodes and translational degrees of freedom (nodal displacements), respec-tively. Both first and second derivatives of system energy are used in the energy minimization computation, hence it is faster than the standard conjugate gradient method which uses only the first order derivative of system energy as discussed in [46]. The stiffness

matrices of these elements are established based upon interatomic potentials. Similar to the conventional finite element method (FEM), the global stiffness matrix is assembled from element stiffness matrices. Hence, relations between atomic dis-placement and force can be derived by solving a system of equations. The potential energy E of the atomic structure is a function of atomic coordinates as below

$E = E(x1, x2, xn)$, (6)

where xi is the position of atom i, and N is the number of atoms. Noting fi is the external force exerted on atom i, the work of the external forces reads

Eext = z fixi- (7)

The total energy of the atomic structure reads

ET = E- z fim. (8)

The first derivative of the total energy ET for the atomic displacements must be zero because the total energy ET is minimal when the structure is in equilibrium

$R(x) = 0$, (9)

where

Fig. 3. Element types used in the finite element modeling: (a) 3-node element; (b) 4-node element.

Table 1

Sheet lengths in Á after relaxation at 0 K. Every sheet contains 4032 atoms.

3. Results and discussion

Although the present work focuses mainly on tensile properties of pristine and defective BN and SiC sheets, and uniaxial tensile properties of pristine and defective graphene sheets have been well reported in the literature (see e.g. [44,45,52-55]), additional MD and MDFEM simulations with optimized Tersoff potential by Lindsay and Broido [56] are here carried out for pristine

graphene sheet in order to compare with BN and SiC ones as well as demonstrate the accuracy of the MDFEM. MD simulations results of BN and SiC sheets are extracted from Ref. [21]. MD simulations of graphene are performed by LAMMPS code [57] with the same procedure in [21]. o and £ are denoted as the nominal axial stress (engineering stress) and the nominal axial strain (engineering strain), respec¬tively. Young's modulus Y is determined from the first derivative of the stress-strain curve at £ = 0. Only data with £ r 5% is collected for the evaluation of Young's modulus. 2D Young's modulus (or in plane-stiffness) Ys is adopted here and defined as Ys=Yt. t is the sheet's thickness. Uniaxial tensile stress-strain curves obtained by MDFEM and MD simulations coincide closely up to fracture points as shown in Fig. 4. Deviations in Young's modulus obtained by MDFEM and MD simulations are less than 5% as indicated in Table 2. For simple, mesh in MDFEM is generated with the bond length estimated by previous MD simulations [21] after relaxation at 0 K. This mesh is not taken from the relaxed configuration by MD simulations. This simplification may lead to small deviations in uniaxial tensile stress-strain curves up to fracture points and in Young's modulus. It should be noted that MDFEM and MD simulations have used the same interatomic potentials for each sheet. In MD simulations by Le [21] the small cutoff distance was extended to the large one, namely, Rij=Sij; whereas the cut-off function is removed in the present MDEFEM study, fC(rij) = 1, as	

reported in Section 2.2. Hence, artificial raise of bond force (see Fig. 2), and then overestimation in fracture stress could be avoided in both MD simulations [21] and MDFEM. In MD simulations, fracture may occur artificially earlier than expectation because the cutoff function is shifted to a bond strain less than 50% as cited in Section 2.2. Atomic interactions are artificially stopped when bond strain exceeds the shifted value in the cutoff function, although

Fig. 4. Comparisons of uniaxial tensile stress-strain curves obtained by the MDFEM and MD simulations for (a) graphene, (b) BN sheet, and (c) SiC sheet. The sheets are pristine; see the text for detail.

their interactions may prolong in reality well beyond this shifted bond strain. Thus, under tension, MDFEM with the removal of cutoff function may provide more realistic results and higher facture stress and strain than that in MD simulations [21] as shown in Table 2.

Engineering stress and strain are used here, excepting that results from Refs. [52,53] listed in Table 2 are Cauchy stresses for graphene. Poisson's ratio of graphene decreases monotonously from ~ 0.07 during tension. In the present study, engineering stress is almost equal to Cauchy stress for graphene due to low Poisson's ratio. It depends clearly on the used force field para-meters for graphene [56]. Young's modulus and fracture stress of graphene estimated by MDFEM agree very well with those evaluated by DFT calculations [52,53] and by experiment [58] as shown in Table 2. Results on tensile properties of graphene support the accuracy of our MDFEM. Due to the removal of the

cutoff function, MDFEM provides more accurate fracture stress of the armchair graphene sheet than that by MD simulations with the same force field as clearly seen in Table 2. Fracture strain of graphene is close to and lower than that predicted by DFT calculations [52,53] in the armchair and the zigzag directions, respectively.

Young's modulus of pristine BN sheet is about 258 N/m in the zigzag direction and 251 N/m in the armchair one. These values are in good agreement with those by DFT calculations [7,9-12], and by the objective MD study [59]. Assuming a nominal thickness of the sheet t = 3.35 Á, Young's moduli predicted by MDFEM for BN sheet are about 770 GPa (zigzag direction) and 749 GPa (armchair direction), which are close to that of 776 GPa, estimated by inelastic X-ray scattering measurements for single-crystalline hexagonal BN [24]. Young's moduli of pristine SiC sheet predicted by MDFEM are 174 N/m in the zigzag direction and 171 N/m in the armchair one, being 3-7% higher than those estimated by DFT calculations [9,12]. MDFEM estimates fracture stresses at 37.7 and 35.5 N/m for BN sheet, and 20.7 and 17.9 N/m for SiC one, in the zigzag and armchair directions, respectively. Compared to gra-phene [58], hexagonal BN and SiC sheets exhibit approximately 76% and 51% in Young's modulus, and 90% and 49% in fracture stress in the zigzag direction, respectively.

2 types of the Stone-Wales defects and 2-atom vacancy are considered in the present study as schematically illustrated in Fig. 1. A bond, which is initially perpendicular or makes an angle of 30° to the zigzag direction,

rotates by 90° to the Stone-Wales defect type 1 (SW1) or type 2 (SW2), respectively. One 2-atom vacancy is created by removing 2 adjacent atoms. Defective sheet considered here contains only a single defect (one 2-atom vacancy, or SW1 or SW2) in its center. Defect fraction (percentage of number of missing atoms) is relatively low, ~ 0.05%, for the case of one 2-atom vacancy. Uniaxial tensile stress-strain curves of defective and pristine BN sheets are almost identical up to fracture points as shown in Fig. 5. Similar phenomena are also observed for SiC sheets. Hence, the sheet with a single defect exhibits a similar elastic nature to its corresponding pristine one, excepting that fracture occurs earlier in defective one than in pristine one. This phenomenon has been previously observed in graphene and carbon nanotubes by MM [44,45] and MD simulations [54,55].

Fracture occurs at the boundary in pristine sheets under tension as shown in Fig. 6. A hole enlarges from the defect location during the sheet's tension as indicated in Fig. 7 for sheets with 2-atom vacancy. As summarized in Table 3, most of defective sheets experience their fracture at the defect location, excepting that fracture takes places at the boundary in BN sheets with SW1 under tension in the zigzag direction, and with SW2 under tension in the armchair one. All sheets with vacancy break down at the defect location since missing atoms weaken naturally the struc-ture. In contrast, the number of atoms remains unchanged in sheets with Stone-Wales defects. Hence, the sheet is less wea-kened by the Stone-Wales defect than by a vacancy

of 2 missing atoms. The involved bond of SW1 (red bond in the right side of Fig. 1a) and SW2 (red bond in the right side of Fig. 1b) is parallel to the zigzag direction and makes an angle of 30° to the armchair one, respectively. Thus, SW1 and SW2 contribute to the sheet's strength in the zigzag direction and the armchair one, respectively, and reduce the possibility of fracture at defect location under tension in the corresponding direction. At small strains, Poisson's ratios are estimated by MDFEM to be about 0.29 and 0.18 for BN and SiC sheet, respectively. During tension, the sheet length in the transverse direction reduces much in BN sheet than that in SiC

Table 2
Tensile mechanical properties of pristine sheets by various methods. Engineering stress and strain are used, excepting that cited results from Refs. [52,53] are Cauchy stresses; see the text for detail.

Fig. 5. Stress-strain curves of pristine and defective BN sheets under uniaxial tension in the (top) zigzag direction and (bottom) armchair one.

sheet. Consequently, BN sheets with SW1 and SW2 exhibit the fracture at the boundary when stretching in the zigzag and armchair directions, respectively, and this phenomenon is not observed in SiC sheets with SW1 and SW2. It should be empha-sized that Tersoff and Tersoff-like potential parameters for BN [34] and SiC [35] provide not very accurate Poisson's ratios (at small strain, 0.29 for BN sheet and 0.18 for SiC sheet) compared to those by DFT calculations [9,11], 0.21—0.22 and 0.29 for BN and SiC sheet, respectively.

To make Figs. 6 and 7 more visible,

some conventions should be adopted as follows: a bond is plotted in red and not drawn if its length exceeds the large cutoff distance Sij in Eq. (1c) and twice its initial length, respectively. Concerning the pristine SiC sheet under uniaxial tension in the zigzag direction, failure is not found up to its ultimate tensile strain eu=24.8% (strain at maximal stress), but evidently observed at tensile strain e=25.0% as clearly shown in

Table 3

Tensile mechanical properties of pristine and defective sheets.

Fig. 6. A similar phenomenon is observed for other cases. Hence, BN and SiC sheets exhibit brittle fracture with fast fracture process and a drop in the stress—strain curve. It should be noted that ultimate strain (strain at maximal stress) is lower than fracture strain at which the material is completely broken down for ductile materials. Here, all sheets exhibit brittle fracture. Ultimate strain and fracture strain are approximately equal. For example, ultimate and fracture strain of the zigzag pristine SiC sheet are estimated at 24.8% and ~ 25%, respectively. Therefore, ultimate strain can be considered as fracture strain in the present work.

Comparisons of tensile properties of pristine and defective sheets are also given in Fig. 8 and Table 3. Young's modulus of defective sheets reduces within 1.5% from that of corresponding pristine ones. In contrast, one 2-atom vacancy in the sheet's center reduces 15—18% and 16—25% in fracture stress, and 32—34% and 32—48% in fracture strain of BN and SiC sheets, respectively. Reduction in fracture

properties depends on the tensile direction as well as the orientation of Stone—Wales defects. The involved bond in SW1 (red bond in Fig. 1a at the right hand side) is parallel to the zigzag direction, whereas the one in SW2 (red bond in Fig. 1b at the right hand side) makes an angle of 60° to the zigzag direction. Hence, SW1 resists the tension in the zigzag direction better than SW2, whereas SW1 supports the sheet under tension in the armchair direction less than SW2.

Consequently, when stretching in the zigzag direction, fracture properties are less reduced by SW1 than by SW2, while SW1 causes higher reduction in fracture properties than SW2 for defective sheets under tension in the armchair direction. Overall, the Stone—Wales defect reduces fracture stresses about 7—17% and 5—28% for BN and SiC sheets, respectively.

Significant reductions in fracture stress and strain with very slight decrease in Young's modulus due to low defect fraction have been also reported by MM [44,45] and MD simulations [54,55] for graphene and carbon nanotubes. For example, MM simulations by Zhang et al. [44] and Khare et al. [45] showed that a single defect (one- or two-atom vacancy) causes a reduction in the fracture stress of various carbon nanotubes by 20—33%. These reductions

Fig. 8. Fracture stress (top) and fracture strain (bottom) ofpristine and defective sheets.

are 52-61% for fracture strain of (5, 5) and (10, 0) carbon nanotubes. It should be noted that the cutoff function in REBO potential was removed from their MM model. This removal of the cutoff

function is also adopted here as mentioned in Section 2.2. MD simulations with the Tersoff-Brenner potential at 300 K by Chowdhury et al. [54] showed that a missing atom causes a reduction of 15% in fracture stress and 31% in fracture strain of a single-walled (10, 10) armchair nanotube with 500 atoms. There-fore, our results on BN and SiC sheets reflect similar features of graphene-like structures.

4. Summary and concluding remarks

The uniaxial tensile mechanical behavior of pristine and defec-tive BN and SiC sheets under the armchair and zigzag directions is investigated through MDFEM. In the present study, defective sheet contains in its center only a single defect under the form of one 2- atom vacancy, or a Stone-Wales defect type 1, or a Stone-Wales defect type 2. It is found that uniaxial tensile stress-strain curves of defective and pristine sheets are almost identical up to fracture points. A single defect reduces significantly fracture stress and fracture strain from those of the corresponding pristine sheet, whereas Young's modulus is nearly unchanged by a single defect. One 2-atom vacancy reduces 15-18% and 16-25% in fracture stress, and 32-34% and 32-48% in fracture strain of BN and SiC sheets, respectively. Reduction in fracture properties depends on the tensile direction as well as the orientation of Stone-Wales defects. A Stone-Wales defect reduces fracture stresses about 7-17% and 5-28% for BN and SiC sheets, respectively.